

Rare-metal Free Tunneling Magnetoresistance Phenomenon Arising From Edge Spins of Magnetic Graphene Nanopore Arrays

Taijyu Hashimoto¹, Syota Kamikawa¹, David Soriano², Jesper Goor Pedersen^{2,3}, Stephan Roche^{2,4}, Junji Haruyama^{1*}

¹ Faculty of Science and Engineering, Aoyama Gakuin University, 5-10-1 Fuchinobe, Sagamihara, Kanagawa 252-5258, JAPAN

² Institut Català de Nanociència i Nanotecnologia (ICN2), Campus de la UAB, Edifici ICN2, 08193 Bellaterra, Barcelona, Spain

³ DTU Nanotech – Department of Micro-and Nanotechnology, Technical University of Denmark, DK-2800 Kongens Lyngby, Denmark

⁴ ICREA - Institutio Catalana de Recerca i Estudis Avancats, 08010 Barcelona, Spain

*Corresponding author, email : J-haru@ee.aoyama.ac.jp

The advent of spintronics, rooted in the discovery of giant magnetoresistance and tunneling magnetoresistance, has massively impacted on the development of magnetic data-recording technologies and also non-charge-based energy-dissipationless information technologies¹⁻¹⁵. However, using magnetic rare-metals is facing serious problems for the environmental contamination and the limited material-resource. In contrast, by fabricating ferromagnetic graphene nanopore arrays (FGNPAs)^{16-19, 35-39} with hydrogenated zigzag-type atomic structure of nanopore edges, we previously proved presence of spontaneously polarized electron spins driven by edge states at the pore edges^{16,17,20-30}, bringing intrinsic flatland-ferromagnetism in graphenes free from magnetic rare-elements. Here, we demonstrate observation of tunneling magnetoresistance (TMR) behaviors on the junction of FGNPA/SiO₂/cobalt electrode²⁰⁻³¹. We find gradual change in TMR ratios across zero-magnetic field. It is also revealed that the TMR ratios can be controlled by modulating spin current through the hydrogenated FGNPAs arising from spin-orbit interaction by applying back-gate voltage^{14,15,40} and by modulating interpore distance. Theoretical calculation clarifies that the polarized edge spins can tunnel through SiO₂ barrier to the cobalt electrode and cause the unique TMR behaviors, depending on specified spin alignment of the pore edges^{32-34,39,41,42}. Moreover, we find that annealing of the FGNPA/SiO₂ junction drastically improve TMR ratios (~100 %), resulting in realization of room-temperature operation of TMR devices⁴³⁻⁴⁵. An edge-spin-based all-carbon TMR junction must pave the way not only for zero-emission energy but also for rare magnetic-atom free spintronics, resolving the aforementioned problems.

Several key components of spintronics have been realized in recent years, e.g., giant magnetoresistance (GMR), tunneling MR (TMR), and spin valve devices¹⁻⁵. Giant TMR ratios, $(R_{AP}-R_P)/R_P$, where AP and P refer to antiparallel and parallel orientations of the spin configurations of the two electrodes, of ~1000% have been obtained in CoFeB/MgO/CoFeB junctions⁵. A wide variety of materials have been utilized for spintronic devices, such as ferromagnetic metals, e.g., cobalt (Co), iron (Fe), chromium (Cr), and manganese (Mn)¹⁻⁵, as well as

ferromagnetic semiconductors, e.g., (In, Mn)As⁶⁻¹¹. In all cases, however, rare magnetic elements are essential to provide polarized spins to the systems.

In contrast, it is theoretically predicted that graphene edges with certain atomic structures (the so-called zigzag edge; Fig. 1b) are spontaneously spin polarized, exhibiting flat band ferromagnetism, caused from high density of spin states (i.e., the edge states) as well as a strong spin interaction among the localized electrons²⁰⁻²⁷. Importantly, this occurs despite the absence of rare magnetic elements, considering just carbon atoms with sp^2 orbitals²⁰⁻²². In the case of graphene nanoribbons (GNRs; quasi-one-dimensional ribbons of graphene with two edges along those longitudinal directions on both sides; Fig. 1)^{20,27}, the appearance of the spin polarization (e.g., AP for anti-ferromagnetism and P for ferromagnetism) is highly sensitive to the spin interaction between the two edges, and is determined so as to maximize exchange energy gain (similar to Hund's rule in atoms). In particular, spin ground states in GNRs under absent magnetic fields are still under debating stages^{16, 20-23}. Theoretical studies have also suggested that perforated graphene sheets, with pores that induce a sublattice imbalance, are magnetic, with a total magnetic moment determined by Lieb's theorem^{16, 28-30}. Even for pore shapes that preserve sublattice balance, local spin polarization is expected along zigzag edges of the hole, with a spin texture closely reminiscent of zigzag GNRs⁴¹. These properties suggest that novel types of spin-based devices may be realized using graphene-based materials, without the need of rare magnetic atoms³⁰. Long spin diffusion lengths¹³, and the introduction of the colossal spin-orbit interaction by hydrogenation^{14,15,40} are further recent examples of the potential of graphene spintronics.

In prior works^{16,17,39}, we have experimentally confirmed the formation of flat-band ferromagnetism in hydrogen(H)-terminated zigzag-edged GNPAs, which consist of honeycomb-like arrays of hexagonal nanopores on graphene corresponding to a large ensemble of H-terminated zigzag-edged GNRs in the interpore regions (Fig. 1; supplementary materials (SM))^{18,19}. Observation of the significant reduction of the I_G/I_D peak ratios by the critical-temperature annealing (~800 °C) in Raman spectrum and the comparison with previous other experiments (e.g., extremely low I_G/I_D peak ratios in the intentionally fabricated zigzag-edge hexagonal pores³⁴ and in the zigzag-edged graphene flakes³⁵, atomic

reconstruction to zigzag edge by Joule heating³⁶ and electron beam irradiation³⁷) implied formation of the zigzag-type atomic structure of the pore edges by the reconstruction of the edge atomic structure. Moreover, observation of the ferromagnetism induced by decreasing the interpore distance (i.e., width of the interpore GNR regions; Fig. 1)¹⁶ and of the high density of the polarized spins at the pore edges by magnetic force microscope in the ferromagnetic GNPs (FGNPs)¹⁷ suggested that the observed ferromagnetism was attributed to presence of the polarized spins existing at the pore edges. Two theoretical analysis (GNR theory and Lieb's theorem) of the observed magnetization values ($\sim 0.3\mu_B$ /edge dangling bond) also suggested that the mono-hydrogenated zigzag pore edges were the origin for the ferromagnetism¹⁶. The edge states were also confirmed by observation using ionic liquid gate³⁹.

In the present study, TMR junctions utilizing such FGNPs are realized for the first time. The fabricated TMR junction consists of Co/SiO₂/FGNPA (Figs. 2a and 2b), serving as a prototype structure for rare-metal free graphene-based TMR. The honeycomb-like array of hexagonal nanopores forming the FGNPA is shown in the atomic force microscope image (Fig. 1a) and in a schematic view (Fig. 1b). Fabrication followed our previously developed non-lithographic method^{16,17} (see Methods and SM), which realized the low defects and low contamination of the pore edges.

The fabricated TMR structure using this FGNPA as one-side electrode with the optical microscope is shown in Fig. 2a (top-view), and is schematically described in Fig. 2b (also see Methods). The TMR behavior is measured along the constant current path illustrated in Fig. 2b. The TMR ratio is defined as the difference between the resistance values (R_B) at individual magnetic fields (B) and the minimum MR value (R_{min}), which is assumed to be the best parallel spin alignment between Co electrode and FGNPA; i.e., $TMR \text{ ratio} = (R_B - R_{min})/R_{min}$. A magnetization measurement of the overlaid structure of the SiO₂/FGNPA is shown in Fig. 2d. It implies the persistence of the ferromagnetic signal even after evaporation of the SiO₂ film on the pore edges, although the magnitude is reduced somewhat compared with that without SiO₂ film.

Figure 3 gives the result of a typical TMR measurement of the Co/SiO₂/FGNPA junction (shown in Figs. 2a and 2b) under in-plane parallel magnetic field (B) at (a) 1.5K and (b) 300K. We identify the minimum resistance (R_{min}) as the situation in which the external B induces best matching between the spin polarizations of the magnetic materials (i.e., parallel spin alignment between Cobalt and FGNPA) and take this as R_P in subsequent calculations of TMR ratios, as mentioned in the figure caption. The observed TMR behaviors in Fig. 3a are significantly different from those of any other conventional TMR junctions. They exhibit the following unique B -dependent characteristics. (1) TMR ratio is tuned by the B and can reach a signal about 20%. (2) The minimum of TMR ratio appears as B approaches to zero in $-B$ region. (3) The TMR ratios increases gradually crossing $B = 0$. (4) The peak of TMR ratio emerges in $+B$ region. A similar

behavior is observed for polarity changes in B , i.e., when sweeping from $+B$ to $-B$, (the black line in Fig. 3). As illustrated in the curves around zero-TMR ratio, the Co/SiO₂/bulk graphene junction (i.e., without the nanopores) shows drastically different behavior, with showing no clear TMR signatures. This suggests that the TMR-like behavior observed in the Co/SiO₂/FGNPA junction is unique to the present TMR structure, and is driven by spin tunneling properties between the Co electrode and the FGNPA. Present reproducibility of the TMR behaviors is over 80 %, because six of seven samples showed similar behaviors to date.

TMR properties observed at room temperature are shown in Fig. 3b. Maximum TMR ratios significantly decreases from $\sim 20\%$ to $\sim 5\%$ and the behaviors become ambiguous compared with those at low temperatures, because ferromagnetism arising from the pore edges is suppressed in the SiO₂/FGNPA at room temperature in contradiction to the large ferromagnetism remained in FGNPs without SiO₂¹⁶. It should be noticed that, nevertheless, TMR behaviors are still observable.

The observed unique TMR behavior can be qualitatively understood by considering the spin alignment between two opposing pore edges of the FGNPA (i.e., two edges of the interpore GNR region in Fig. 1b) and the Co electrode. It also clarifies spin ground states of the H-terminated zigzag-type GNRs under no B . We support these interpretations by atomistic simulations (see Methods and SM). First, we calculate the density of states (DOS) of a GNP reminiscent of the fabricated structure (Fig. 4a). The calculated DOS (Fig. 4b) is compared to that obtained for an infinitely long zigzag GNR corresponding to the structure highlighted in the zoom in Fig. 4a, evidencing a close resemblance of the electronic structures of the two systems. Ignoring the tunnel barrier, the TMR device is thus conveniently visualized as a junction between a spin injector and an array of uncoupled zigzag GNRs, the spin polarizations of which depend on the B . Based on this result, we simulate the spin transport properties of the device via a zigzag GNR-based junction, in which the spin polarization is differentiated between left (Co spin injector) and right (FGNPA) parts (Fig. 4d). We focus on the sweep from $-B$ to $+B$ (red curve in Fig. 3).

As indicated in Figs. 4c and 4d, we identify three distinct regions in the TMR response, corresponding to the situations where the magnetization of the FGNPA (i.e., spin alignment of two edges of the interpore GNRs) is ferromagnetic ($F_{\uparrow\uparrow}$; the two black arrows at the subscript mean the spin moment of two edges of the interpore GNR) with spins parallel to the spin injector (Co) ($F_{\uparrow\uparrow\uparrow}$; the red subscript arrow is the spin moment of injector), anti-ferromagnetic (AF; $F_{\uparrow\downarrow\uparrow}$), and ferromagnetic with spins anti-parallel to the spin injector ($F_{\downarrow\downarrow\uparrow}$). At $-B$, the spins of the injector and the FGNPA are largely parallel ($F_{\uparrow\uparrow}$), resulting in maximum conductance through the junction (Fig. 4c), and thus the minimum of the TMR ratio in Fig. 3. As the B approaches zero, the GNR array (i.e., ensemble of the two edges of the interpore GNRs) gradually transitions to an AF configuration ($F_{\uparrow\downarrow}$), where half of the conductance channels are suppressed, resulting in the half value of conductance (Fig. 4c) and gradual increase in the TMR

ratio ($F_{\uparrow\uparrow}$). As the B is increased further to $+B$, the spin polarization of the GNR array changes to the ($F_{\downarrow\downarrow}$) configuration, suppressing all edge conductance channels, resulting in the conductance minimum (Fig. 4c) and subsequent the peak of TMR ratio observed around $B = 0.5$ T ($F_{\downarrow\uparrow}$). At higher B , the spins of the Co injector start to align with the magnetic field, gradually quenching the TMR ratio, while non-zero TMR ratios in higher B regions suggest instability of the pore edge spins of the FGNPAs.

Note that the exact values obtained in the simulations are specific to the zigzag geometries used in the calculation, and thus cannot be quantitatively compared with experiments. However, the trends observed in Fig. 4c confirm the scenario proposed for the observed TMR behaviour. It implies that the edge polarized spins of the inter-pore GNR regions can tunnel through SiO_2 barrier forming the spin alignment with the spins of Co and also that the spin ground states of the H-terminated zigzag-GNRs are AF under no B . This result is consistent with our previous experimental results, which exhibited ferromagnetism only when B is applied^{16,17}. It is important to note that the main mechanism revealed by our simulations does not depend on how the electrons are really injected from the cobalt electrode to the GNPA, but how efficiently spin-polarized electrons injected on the GNPA are further transmitted depending on the magnetic ordering of the local moments along the zigzag edges.

Here, we also demonstrate that the TMR characteristics can be controlled by changing a back gate voltage (V_{bg} ; Fig.2b) (Figs. 5a and 5b), as well as to the inter-pore spacing (W ; i.e., width of inter-pore GNRs in Fig. 1) (Figs. 5c and 5d). The TMR ratio exhibits a maximum value of $\sim 20\%$ at $V_{\text{bg}} = +30\text{V}$ (Figs. 3, 5a, and 5b), while it is reduced with decreasing V_{bg} toward $-V_{\text{bg}}$ region (Figs. 5a and 5b). This is consistent with the presence of evident spin-based phenomena observed only at $V_{\text{bg}} = +30$ V for previous in-plane measurements of MR behaviors of FGNPAs¹⁶. One qualitative interpretation for these V_{bg} dependence is influence of the spin-orbit interaction (SOI) introduced into the FGNPA by the H-terminated pore edges, because the Au electrode was placed at the side position of the Co/ SiO_2 /FGNPA junction and the in-plane spin current path exists through the FGNPA to the Au electrode (Fig. 2b). Conventionally, graphene has no SOI because of the small mass. In contrast, introduction of the colossal SOI (e.g., spin relaxation time of ~ 90 ps and a SO strength of $\sim 2.5\text{meV}$ in 0.01%-hydrogenated graphene), which originates from the formation of sp^3 bond by hydrogenation and the broken symmetry along z -axis (out-of plain) direction (i.e., Rashba-type SO scattering), and the spin-Hall Effect (SHE) were recently reported in graphenes precisely hydrogenated by utilizing a hydrogen Silsesquioxane (HSQ) resist¹⁴. We have also reconfirmed it with strong interaction with spin phase interference phenomena³⁸. Also in the present FGNPA, hydrogenated-inter-pore GNR regions and H-terminated pore edges⁴⁰ should introduce similar sp^3 bonds and induce the SOI.

Following ref. 14, we carried out HSQ resist treatment in the GNPA and measured magnetization ($SM8$)⁴². Result of the linear relationship for the saturation magnetization

value vs. the hydrogen volume is confirmed in Fig. 5e (dotted line). We could attain magnetization values in the HSQ-GNPAs with 0.06%-hydrogenation at least a few-ten-times greater than those in the present non-HSQ FGNPAs, which was H-terminated only at high-temperature annealing under H_2 atmosphere. These results imply that the edge dangling bonds have been certainly H-terminated, leading to the enhancement of the ferromagnetism and the introduction of SOI. The magnetization value in Fig. 5e suggests that the volume of the hydrogenation in the present non-HSQ FGNPAs corresponds to 0.005%. In ref.14, magnitude of the SHE became mostly a half value in the samples from 0.01% to 0.005% H-volumes. It suggests that magnitude of the spin current also becomes a half value and, hence, spin relaxation length l_s of ~ 2 μm , a spin relaxation time of ~ 200 ps and a SO strength of ~ 1.25 meV can be estimated in the present non-HSQ FGNPAs under in-plane magnetic field, when the influence of spin scattering by the pore edges and the enhancement of SOI by H-termination⁴⁰ are not considered. Here, length of the in-plane spin current path through the FGNPA to the Au electrode (i.e., the lateral space between Co and Au electrodes in Fig. 2b) is ~ 1 μm . Because this value is smaller than the aforementioned l_s of ~ 2 μm , spin current arising from SOI in the 0.005%-H area by applied V_{bg} can directly contribute to the TMR behavior by the spin alignment as explained above.

When V_{bg} is applied as perpendicular (out-of plane) electric fields, spin current appears via. the SOI. If the spin moment of the spin current (SOI_{\downarrow}) which is parallel to those in the FGNPAs dominates (e.g., $\text{SOI}_{\downarrow} + F_{\downarrow\uparrow}$), it leads to the increase in the TMR ratio peak (i.e., those in $+V_{\text{bg}}$ region). In contrast, when $-V_{\text{bg}}$ is applied, the opposite-moment spin dominates resulting in the anti-parallel spin alignment ($\text{SOI}_{\uparrow} + F_{\downarrow\uparrow}$) and, hence, it reduces the TMR ratio peak.

For larger inter-pore spacing of $W \sim 40$ nm, the TMR value further decreases significantly (Figs. 5c and 5d). For such a large spacing, the spin polarization of opposing pore edges (i.e., two edges of inter-pore GNRs) becomes unstable due to suppressed spin interaction, quenching the TMR properties. TMR ratios also decrease when using FGNPAs with smaller W (Figs. 5c and 5d), because $W \leq 20$ nm is too narrow to form spin currents along the in-plane current path through the FGNPA to Au electrode (Fig. 2b). Although ferromagnetism is stronger for smaller W ¹⁶, induced scattering by the nanopore array heavily obstructs spin flow to the Au electrode, reducing the TMR ratio. This is again consistent with previously observed spin-based phenomena in FGNPAs with $W \sim 30$ nm¹⁶. Therefore, the optimum W value exists for the TMR ratios.

We have reported unique TMR behaviors in the Co/ SiO_2 /FGNPA junctions, nevertheless the maximum TMR ratio is as low as $\sim 20\%$ (Fig. 3a). One of the reasons is the poor interaction at the SiO_2 /FGNPA interface, particularly at the pore edges, which destructs transport of the spin-alignment current and reduces TMR ratios. In contract, as shown in Fig. 6a, we find that annealing of the SiO_2 /FGNPA structure at ~ 500 $^\circ\text{C}$ right after the deposition of SiO_2 tunneling layer drastically (i.e., $> \sim 5$ times)

improves the TMR ratios shown in Fig. 3, which was the result of the junction without annealing. At room temperature, the maximum TMR ratio increases even by ~10 times (Fig. 6b) compared to that in Fig. 3b.

It is known that electronic transport in graphene is highly sensitive to interaction of graphene with the SiO₂ substrate⁴³⁻⁴⁵. The interaction significantly reduces electron mobility in some cases, whereas charge transfer occurs in other cases. The origin depends on termination of SiO₂ surface such as Si-, O-, and H-terminations, as follows⁴³. In the case of Si-terminated surface, interaction between graphene and SiO₂ is very weak resulting in no carrier doping and Fermi level lies at the Dirac point. In contrast, O-termination induces the interaction, leading to a binding energy of C-O bond increasing to 0.78 eV per C atom and a small gap of 0.13 eV at the Dirac point and hole doping (p-type semiconducting behavior). If one of the two dangling bonds at each surface Si atom is terminated by H atom, the interaction at graphene/SiO₂ interface is also induced by enhancement of binding energy of 0.18 eV per C atom, leading to electron doping. In our SiO₂/FGNPA junction, SiO₂ tunnel barrier was deposited on H-terminated FGNPA. However, similar interaction can be qualitatively assumed, determining the interaction between the partially H-terminated pore edges of FGNPA and SiO₂ layer. It also determines strength of the tunnel current and TMR ratios. Our FGNAs show n-type behavior before SiO₂ deposition¹⁶ and the behavior is enhanced after SiO₂ deposition and the annealing. This means that our case corresponds to the H-terminated SiO₂ surface as mentioned above. This suggests that H atoms terminating the pore edge dangling bonds were partially used for termination of one of the two dangling bonds at Si atom of SiO₂ layer by the annealing, leading to enhancement of the electron transfer from SiO₂ layer to graphene with Fermi-level alignment and to an increase in the tunnel current with spin alignment. Therefore, the TMR ratios are significantly improved, even at room temperature (Fig. 6b).

This promises that introducing a lattice-matched tunnel barrier layer (or using thin films of MgO or Al₂O₃) instead of SiO₂ and also improvement of magnitude of the ferromagnetism in the SiO₂/FGNPA junction (e.g., utilizing HSQ resist treatment as mentioned above) can increase TMR ratios further toward ~1000 % order and make evident room-temperature operation possible. Moreover, replacing the Co electrode by another FGNPA must significantly improve the performance of the TMR behaviors at room temperature.

Methods

Fabrication of the FGNPA TMR device (see also SM)^{16,17}. We have used mechanically exfoliated graphene, which was carefully etched using a nanoporous alumina template as a mask. The structure was subsequently annealed under high vacuum and hydrogen atmosphere at critical temperatures (800 °C). Atomic reconstruction of the pore edges during the annealing process resulted in mono-hydrogenated zigzag pore edges with very little disorder. After formation of the FGNPA, Au/Ti four-probe electrodes were fabricated, followed by evaporation of a

10nm thin SiO₂ tunnel barrier on the entire FGNPA. A Co electrode was then evaporated on top of the SiO₂/FGNPA structure, resulting in the formation of the (Co/SiO₂/FGNPA) TMR structure.

Theoretical simulations. The simulations are based on a nearest-neighbor tight-binding model of graphene, including a single π -orbital for each carbon atom. The density of states (DOS) is calculated using the kernel polynomial method³³, via an expansion in Chebyshev polynomials, approximating the trace operation via an initial random phase state, and employing the Jackson kernel. Calculations for the FGNPA DOS are performed on a supercell containing roughly 16 million carbon atoms. For the spin-dependent transport simulations we employ a tight-binding model containing an exchange interaction term that allows for different magnetic configurations at the zigzag edges (see Supplementary Material). Conductance traces are calculated via the Landauer-Büttiker formalism, using a standard decimation technique to treat the semi-infinite ZZ GNR leads.

References

1. Baibich, M. N., Bruto, J. M., Fert, A. Giant Magnetoresistance of (001)Fe/(001)Cr Magnetic Superlattices. *Phys. Rev. Lett.* **61**, 2472 (1988).
2. Binasch, G., Grunberg, P., Saurenbach, F. & Zinn, W. Enhanced magnetoresistance in layered magnetic structures with antiferromagnetic interlayer exchange. *Phys. Rev. B* **39**, 4828 (1989).
3. Moodera, J. S., Kindler, L. R., Wong, T. M. & Meservey, R. Large Magnetoresistance at Room Temperature in Ferromagnetic Thin Film Tunnel Junctions. *Phys. Rev. Lett.* **74**, 3273-3276 (1995).
4. Yuasa, Y., Nagahama, T., Fukushima, A., Suzuki, Y. & Ando, K. Giant room-temperature magnetoresistance in single-crystal Fe/MgO/Fe magnetic tunnel junctions. *Nature Mat.* **3**, 868-871 (2004).
5. Hayakawa, J., Ikeda, S., Lee, Y. M., Matsukara, F. & Ohno, H. Effect of high annealing temperature on giant tunnel magnetoresistance ratio of CoFeB/MgO/CoFeB magnetic tunnel junctions. *Appl. Phys. Lett.* **89**, 232510 (2006).
6. Munekata, H. *et al.* Diluted Magnetic III-V Semiconductors. *Phys. Rev. Lett.* **63**, 1849-1852 (1989).
7. Ohno, H., Munekata, H., Penney, T., von Molár, S. & Chang, L. L. Magnetotransport properties of p-type (In,Mn)As diluted magnetic III-V semiconductors. *Phys. Rev. Lett.* **68**, 2664-2667 (1992).
8. Ohya, S., Kobayashi, H. & Tanaka, M. Magnetic properties of heavily Mn-doped quaternary alloy ferromagnetic semiconductor (InGaMn)As grown on InP. *Appl. Phys. Lett.* **83**, 2175 (2003).
9. Bonanni, A. *et al.* Paramagnetic. GaN:Fe and ferromagnetic (Ga,Fe)N: The relation between structural, electronic and magnetic properties. *Phys. Rev. B* **75**, 125210 (2007).
10. Hai, P. N., Yokoyama, M., Ohya, S. & Tanaka, M.

- Tunneling magnetoresistance of MnAs thin film/GaAs/AlAs/GaAs:MnAs nanoclusters and its AlAs barrier thickness dependence. *Appl. Phys. Lett.* **89**, 242106 (2006).
11. Hai, P. N., Ohya, S., Tanaka, M., Barnes, S. E. & Maekawa, S. Electromotive force and huge magnetoresistance in magnetic tunnel junctions. *Nature* **458**, 489-492 (2009).
 12. Dery, H. *et al.* Nanospintronics Based on Magnetologic Gates. *IEEE Trans. Electron Devices* **59**, 259 (2012)
 13. Abanin, D. A. *et al.* Giant Nonlocality Near the Dirac Point in Graphene. *Science* **332**, 328-330 (2011).
 14. Balakrishnan, J., Koon, G. K. W., Jaiswal, M, Castro Neto, A. H. & Özyilmaz, B. Colossal enhancement of spin-orbit coupling in weakly hydrogenated graphene. *Nature Physics* **9**, 284-287 (2013).
 15. Kane C. L. & Mele, E. J. Quantum Spin Hall Effect in Graphene. *Phys. Rev. Lett.* **95**, 226801 (2005).
 16. Tada, K., Hashimoto, T., Haruyama, J., Yang, H. & Chshiev, M. Spontaneous spin polarization and spin pumping effect at edges of graphene antidot lattices. *Physica Status Solidi B* **249**, 2491-2496 (2012).
 17. Shimizu, T., Nakamura, J., Tada, K., Yagi, Y. & Haruyama, J. Magnetoresistance oscillations arisen from edge-localized electrons in low-defect graphene antidot-lattices. *Appl. Phys. Lett.* **100**, 023104 (2012).
 18. Pedersen, T. G. *et al.* Graphene Antidot Lattices: Designed Defects and Spin Qubits. *Phys. Rev. Lett.* **100**, 136804 (2008).
 19. Bai, J., Zhong, X., Jiang, S., Huang, Y. & Duan, X. Graphene nanomesh. *Nature Nanotech.* **5**, 190-194 (2010); Jung, I., Jang, H. Y. & Park, S. Direct growth of graphene nanomesh using an Au nano-network as a metal catalyst via chemical vapor deposition. *Appl. Phys. Lett.* **103**, 023105 (2013).
 20. Nakada, K., Fujita, M., Dresselhaus, G. & Dresselhaus, M. S. Edge state in graphene ribbons: Nanometer size effect and edge shape dependence. *Phys. Rev. B* **54**, 17954-17961 (1996).
 21. Kusakabe, K. & Maruyama, M. Magnetic nanographite. *Phys. Rev. B* **67**, 092406 (2003).
 22. Fujita, M., Wakabayashi, K., Nakada, K. & Kusakabe, K. Peculiar Localized State at Zigzag Graphite Edge. *J. Phys. Soc. Jpn.* **65**, 1920 (1996).
 23. Son, Y.-W., Cohen, M. L. & Louie, S. G. Half-metallic graphene nanoribbons. *Nature* **444**, 347 (2006).
 24. Son, Y.-W., Cohen, M. L. & Louie, S. G., Energy gaps in graphene nanoribbons. *Phys. Rev. Lett.* **97**, 216803 (2006).
 25. Soriano, D. *et al.* Magnetoresistance and Magnetic Ordering Fingerprints in Hydrogenated Graphene. *Phys. Rev. Lett.* **107**, 016602 (2011).
 26. Yang, H. X. *et al.* Proximity Effects Induced in Graphene by Magnetic Insulators: First-Principles Calculations on Spin Filtering and Exchange-Splitting Gaps. *Phys. Rev. Lett.* **110**, 046603 (2013).
 27. Shimizu, T., Haruyama, J. *et al.* Large intrinsic energy bandgaps in annealed nanotube-derived graphene nanoribbons. *Nature Nanotech.* **6**, 45-50 (2011).
 28. Fürst, J. A., Pedersen, T. G., Brandbyge, M., Jauho, A.-P. Density functional study of graphene antidot lattices: Roles of geometrical relaxation and spin. *Phys. Rev. B.* **80**, 115117 (2009)
 29. Yang, H.-X., Chshiev, M., Boukhalov, D. W., Waintal, X. & Roche, S. Inducing and optimizing magnetism in graphene nanomeshes. *Phys. Rev. B.* **84**, 214404 (2011).
 30. Lieb, E. H., Two theorems on the Hubbard model. *Phys. Rev. Lett.* **62**, 1201-1204 (1989).
 31. Yazyev. O. V., Emergence of magnetism in graphene materials and nanostructures. *Rep. Prog. Phys.* **73**, 056501 (2010)
 32. Muñoz-Rojas, F., Fernández-Rossier, J. & Palacios, J. J. Giant magnetoresistance in ultrasmall graphene based devices. *Phys. Rev. Lett.* **102**, 136810 (2009).
 33. Weisse, A., Wellein, G., Alvermann, A. & Fehske, H. The kernel polynomial method. *Rev. Mod. Phys.* **78**, 275-306 (2006).
 34. Krauss, B., Incze, P. N., Skakalova, V., Biro, L. P., Klitzing, K.von, and Smet, J. J. Raman Scattering at Pure Graphene Zigzag Edges. *Nano Lett.* **10**, 4544 (2010).
 35. You, Y., Ni, Z., Yu, T., and Shen, Z. Edge chirality determination of graphene by Raman spectroscopy. *Appl. Phys. Lett.* **93**, 163112 (2008).
 36. Jia, X., Dresselhaus, M. S. *et al.*, Controlled Formation of Sharp Zigzag and Armchair Edges in Graphitic Nanoribbons. *Science* **323**, 1701 (2009).
 37. Girit, C. O. *et al.*, Graphene at the Edge: Stability and Dynamics. *Science* **323**, 1705 (2009).
 38. Kamijyo, J., Nakamura, T., Haruyama, J. *et al.*, Spin phase interference phenomena associated with spin orbit interaction in hydrogenated graphenes, In-depth-review under *Nature Com.*
 39. Hashimoto, T., Kamikawa, S., Yagi, Y., Haruyama, J., Electronic Properties of Nanopore Edges of Ferromagnetic Graphene Nanomeshes at High Carrier Densities under Ionic-Liquid Gating. *Materials Sciences and Applications* **5(1)**, 1-9 (2014).
 40. Schmidt, M. J. and Loss, D., Edge states and enhanced spin-orbit interaction at graphene/graphane interfaces. *Phys. Rev. B* **81**, 165439 (2010)
 41. Trolle, M. L., Møller, U. S., and Pedersen, T. G., Large and stable band gaps in spin-polarized graphene antidot lattices, *Phys. Rev. B* **88**, 195418 (2013).
 42. Kato, T., Nakamura, T., Haruyama, J. *et al.*, High-Efficiency Graphene Nanomesh Magnets Realized by Controlling Hydrogenation of Pore Edges. Review under *Appl. Phys. Lett.*
 43. Kang, Y.-J., Kang, J., and Chang, K.J., Electronic structure of graphene and doping effect on SiO₂. *Phys. Rev. B* **78**, 115404 (2013).
 44. Jippo, H., Ozaki, T., Ohfuchi, M. First-principles electronic transport calculations of graphene nanoribbons on SiO₂/Si. *Appl. Phys. Exp.* **7**, 025101 (2014)
 45. Nguyen, TC, Otani, M, Okada, S, Semiconducting electronic property of graphene adsorbed on (0001) surfaces of SiO₂, *Phys. Rev. Lett.* **106**, 106801 (2011).

Acknowledgements

The authors thank T. Nakamura, J. Kamiyjo, K. Fujita, Y. Hashimoto, Y. Iye, S. Katsumoto, M. Yamamoto, S. Tarucha, H. Hibino, T. Ando, T. Enoki, M. Koshino, J. Akimitsu, T. Muranaka, Y. Yagi, and M. S. Dresselhaus for their technical contribution, fruitful discussions, and encouragement. This work at Aoyama Gakuin was partly supported by a Grant-in-aid for Scientific Research (Basic research A: 24241046) in MEXT and AFOSR grant. The work by J.G.P. is financially supported by the Danish Council for Independent Research, FTP Grants No. 11-105204 and No. 11-120941. S.R. and D.S acknowledge financial support by the Spanish Ministry of Economy and Competitiveness (MAT2012-33911).

Author contributions

T.H., S.K., S.H, and S.S performed the experiments. D.S. and J.G.P. designed the model and performed the simulations. J.H., D.S, J.G.P and S.R. analyzed the data and wrote the manuscript.

Author information

Reprints and permissions information is available at www.nature.com/reprints. Correspondence and requests for materials should be addressed to J.H. (J-haru@ee.aoyama.ac.jp).

Competing financial interests

The authors declare no competing financial interests.

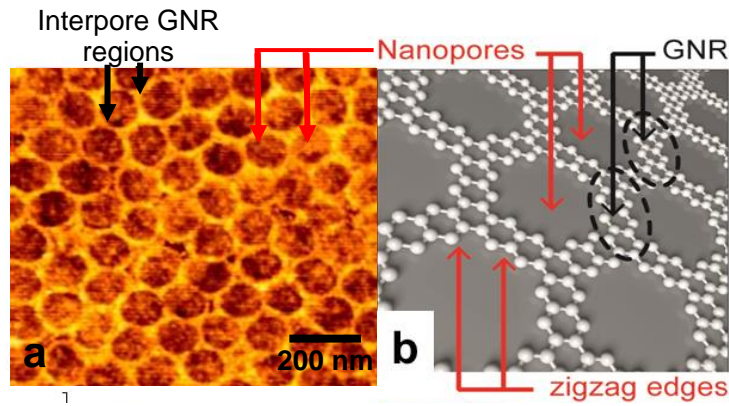


Figure 1 | Characterization of the ferromagnetic graphene nanopore array (FGNPA; see SM). **a**, AFM image of the FGNPA, which consists of a honeycomb-like array of hexagonal nanopores. The typical inter-pore distance is ~ 30 nm, while the pore diameter is ~ 80 nm. **b**, Schematic top view of a GNP with zigzag-type atomic structure at the pore edges. Inter-pore regions correspond to zigzag-type GNRs (e.g. with width of ~ 30 nm), which are one-dimensional strip lines of graphenes. Because the FGNPA corresponds to a large ensemble of the zigzag GNRs, it is effective to detect small magnetic and electric signals arising from the pore edge spins. In actual samples, larger number of carbon unit cells exists in one inter-pore-GNR region.

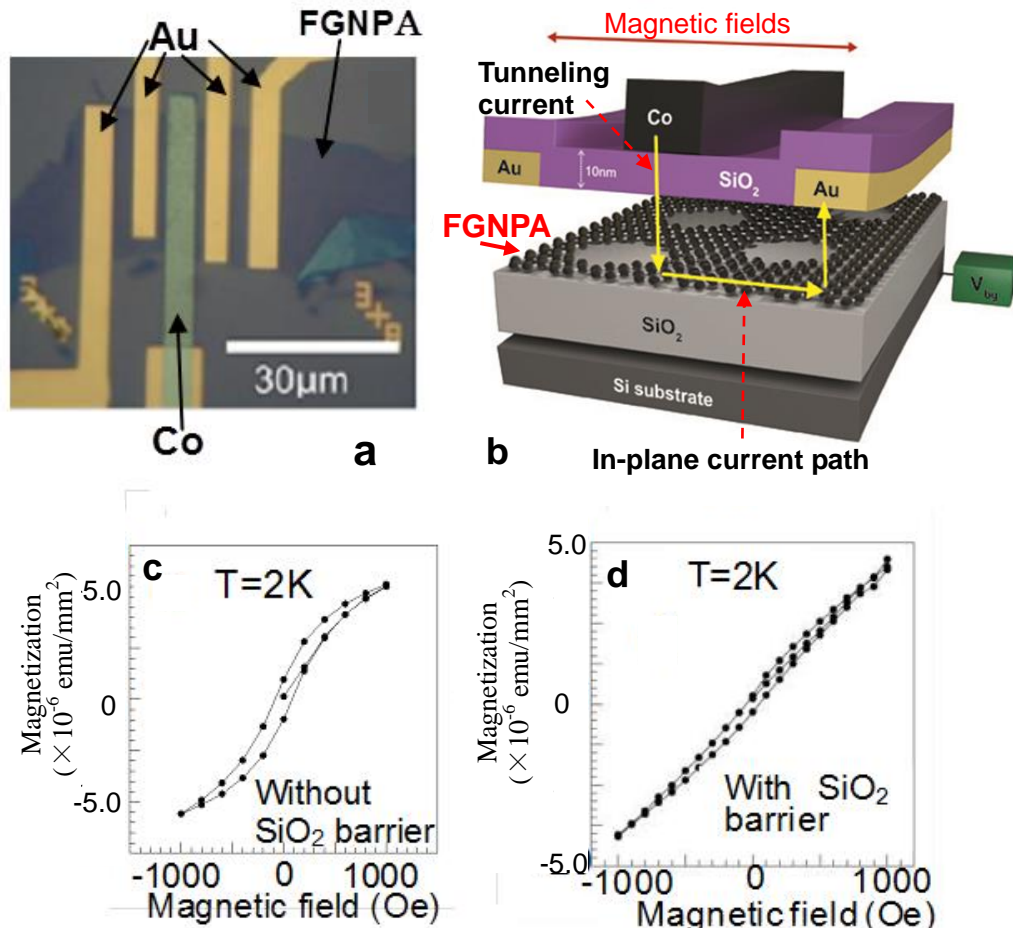


Figure 2 | Structure of the FGNPA-based TMR junction. **a**, Optical microscope image of a top view of the electrode pattern of the TMR junction. MR between the top Co electrode and the Au electrode located at the nearest right side was measured under constant current mode of 1 nA. **b**, Schematic cross section of the TMR junction consisting of Co/SiO₂/FGNPA electrode. The white line illustrates the constant current path. In order to flow into or from Au electrode, spin current must flow through the FGNPA along the lateral current path. Thickness of the SiO₂ tunnel barrier of ~ 10 nm was confirmed by ellipsometry. Magnetic fields were applied in parallel with the FGNPA plane. A back gate voltage (V_{bg}) was applied from the back side of the Si substrate via surface SiO₂ film of Si substrate. **c**, Ferromagnetism observed in mono-hydrogenated GNP without the SiO₂ tunnel barrier layer. The unit area includes the pore area. Accurate estimation of magnetization per pore edge dangling bond was shown in ref. 16. **d**, Ferromagnetism observed in mono-hydrogenated GNP with the SiO₂ tunnel barrier, which results in the TMR junction shown in **b**. Measurements were performed using a DC superconducting quantum interference device of Quantum Design. Note that ferromagnetism, while reduced, remains observable in **d**.

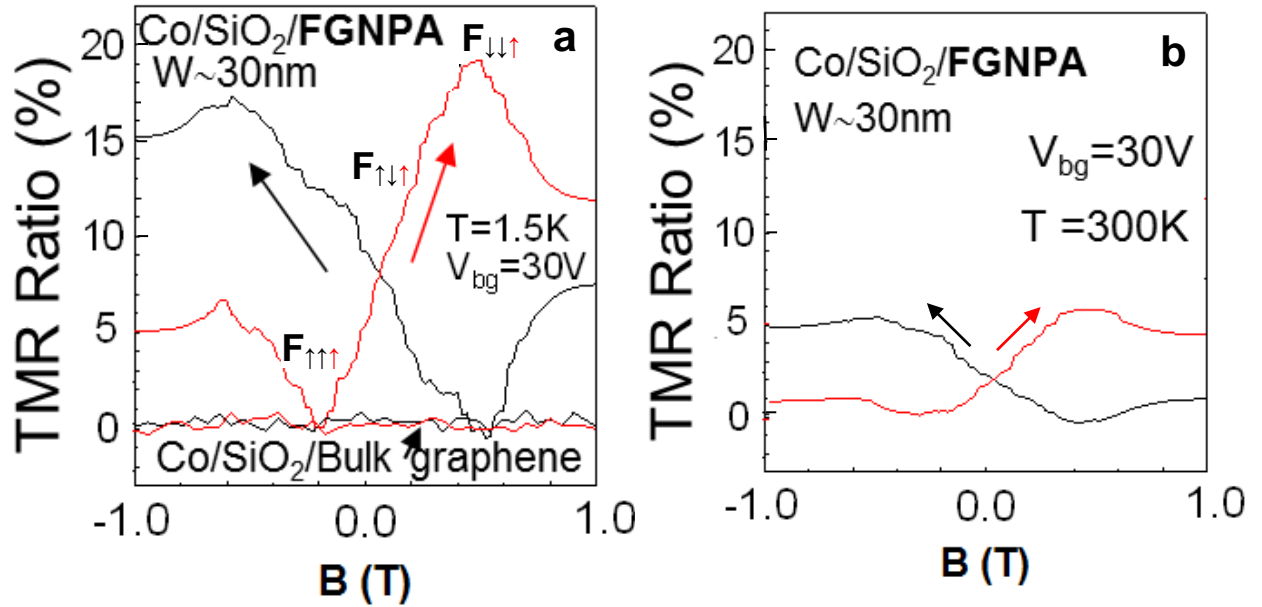


Figure 3 | TMR behaviors of the Co/SiO₂/FGNPA junction without annealing at (a) 1.5K and (b) 300K. Magnetic field sweeps were performed from $B = -1$ to $+1$ T (red line) and $B = +1$ to -1 T (black line). Those shown around mostly constant TMR ratio of zero in (a) are TMR values for the Co/SiO₂/bulk junction. Notation $F_{\uparrow\uparrow}$ means spin configuration of the two edges of an interpore GNR region (left two black arrows) in the FGNPAs and the Co (right red arrow). Gradual changes in TMR ratios for the Co/SiO₂/FGNPA junction are observed around $B = 0$ with the TMR minimum and peak. The TMR minimum corresponds to a ferromagnetic regime with the two edges of an interpore GNR region parallel to the spins of the Co electrode ($F_{\uparrow\uparrow}$) (see Figs. 4c and 4d). Gradual TMR changes across $B = 0$ corresponds to a half-parallel spin alignment regime arising from the anti-ferromagnetic spin configuration of two edges of an interpore GNR ($F_{\uparrow\downarrow}$), while the TMR peak is the ferromagnetic regime, where the FGNPA spins are anti-parallel to the Co spins ($F_{\downarrow\uparrow}$)

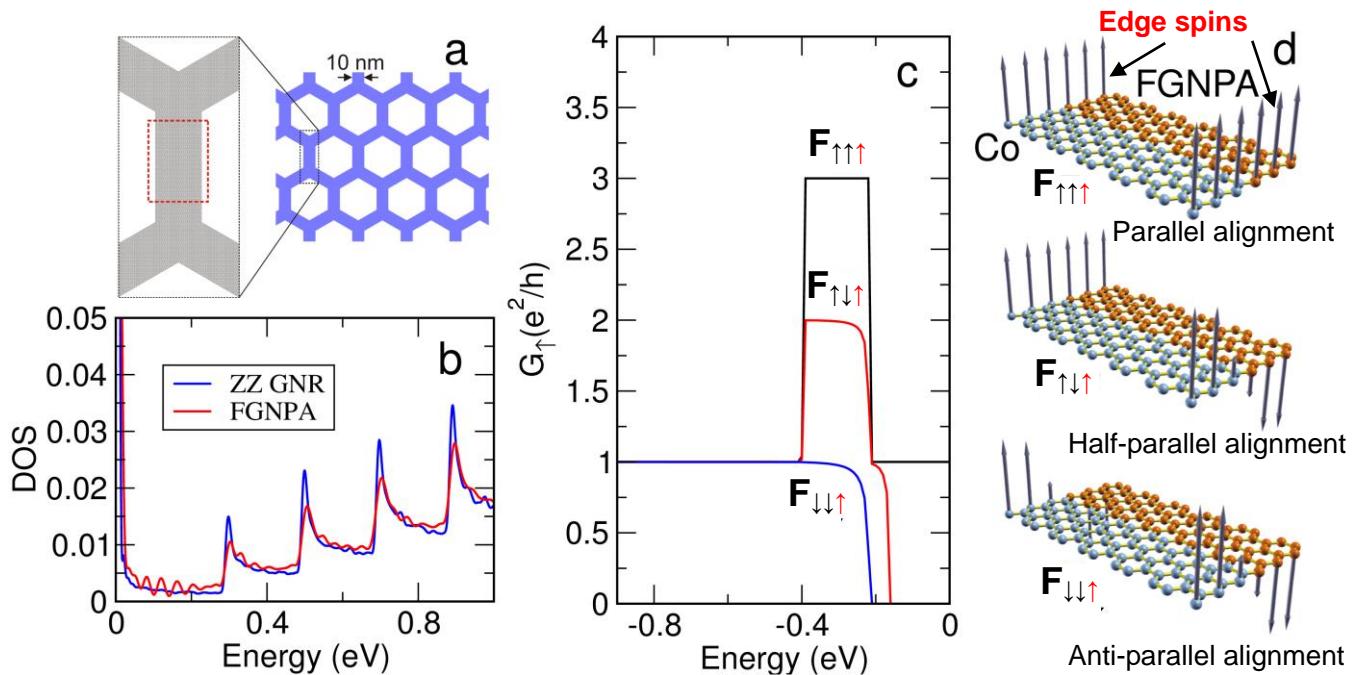


Figure 4 | Calculation results for graphene nanopore electronic structure and spin-dependent tunnel conductance through polarized junctions. **a**, Schematic of a GNPA, used for calculation, with an interpore distance of $W \sim 10$ nm and a pore diameter of ~ 80 nm. Zoom shows the simulated atomic structure, highlighting the correspondence with the interpore zigzag GNRs (red dashed line). **b**, Density of states calculated for the GNPA and the related zigzag GNR. **c**, Conductance between zigzag GNR junctions with different edge spin polarization states and cobalt electrode ($F_{\uparrow\uparrow}$, $F_{\uparrow\downarrow}$, $F_{\downarrow\uparrow}$, see text and Fig. 3). Note the distinct differences in the MR signal in the energy regime where edge states dominate the electronic properties of the GNR. **d**, Spin textures of the corresponding junctions. Yellow and blue parts correspond to the interpore GNR region in a FGNPA and Co electrode, respectively, in the experimental structure. Edge spins in the FGNPA region correspond to those at two edges of an interpore GNR region. Edges spins of cobalt electrode was described to show spin alignment to those in an interpore GNR, although cobalt electrode has actually no specified edge spins.

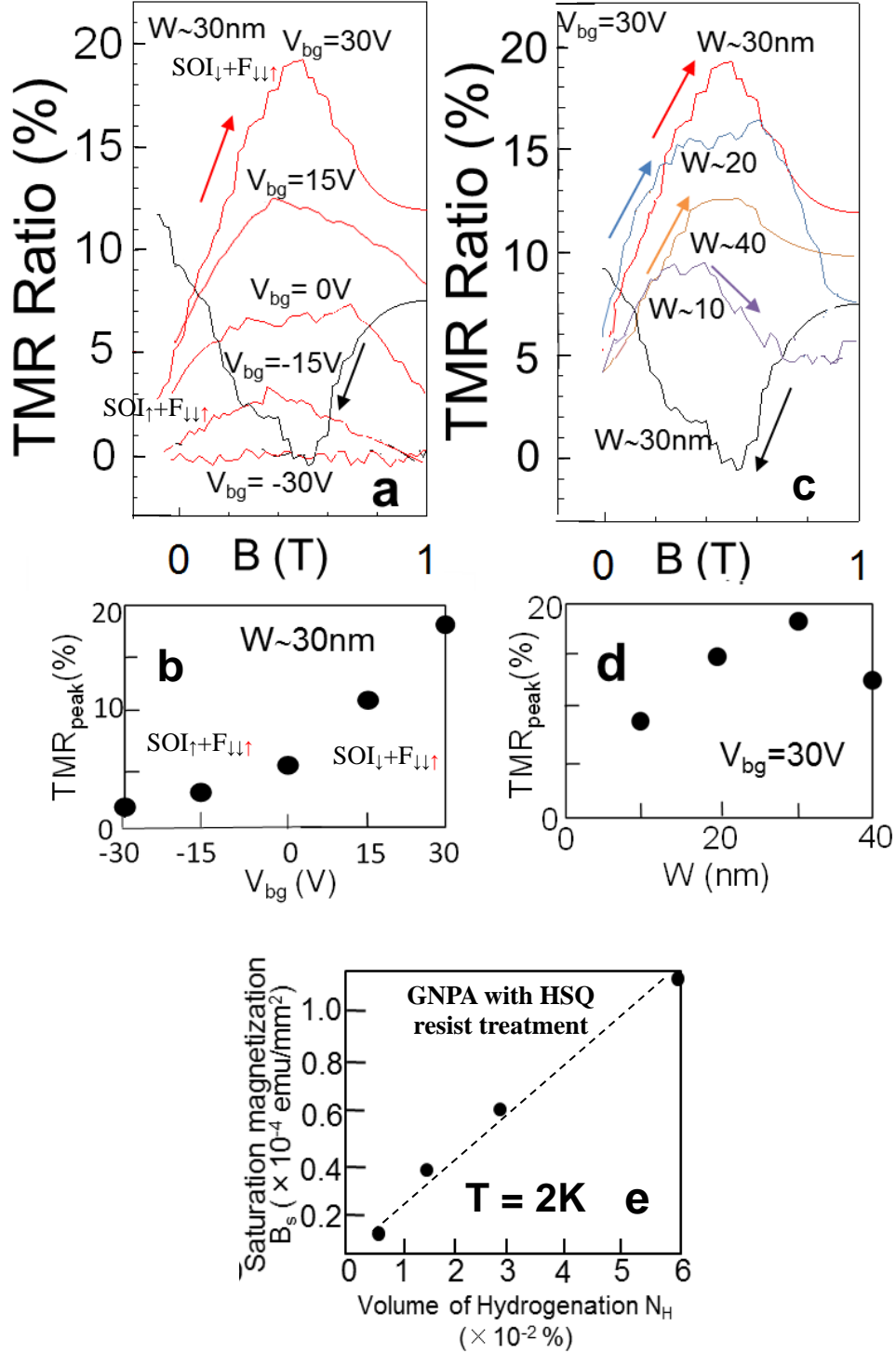


Figure 5 | Back-gate-voltage (V_{bg}) and inter-pore-spacing (W) dependence of the TMR behavior. **a**, Measurements of the sample shown in Fig. 3 for V_{bg} from +30V to -30 V are shown by red curves, while a black line shows that for $-B$ to $+B$ regions for reference. Notation ($SOI_{\downarrow}+F_{\uparrow\uparrow\uparrow}$) means spin configuration of the moment of spin current caused by the V_{bg} -applied SOI in the FGNPAs (SOI_{\downarrow}) and the aforementioned spin alignment of the pore edges and Co ($F_{\uparrow\uparrow\uparrow}$). **b**, V_{bg} dependence of peak values of the TMR ratios shown in Fig. 5a. $-V_{bg}$ and $+V_{bg}$ regions correspond to SOI_{\downarrow} and SOI_{\uparrow} , respectively. **c**, Measurements of a sample similar to that in Fig. 3a but with different W . Exhibited B regions are the same as Fig. 5a. **d**, W dependence of peak values of the TMR ratios shown in Fig. 5c. **e**, **Hydrogenation of GNPA by HSQ resist treatment.** The relationship for the saturation magnetization value vs. hydrogen volume. The dotted line is only guide to eyes. Hydrogen volume was estimated from the I_G/I_D peak ratios in Raman spectrum in our bulk graphenes with the HSQ resist treatment (SM8)^{14,42}. Magnetization values were measured by SQUID (Quantum design) in GNPA with HSQ resist treatment. The present FGNPAs used for the TMR experiments were hydrogenated only under H_2 atmosphere, leading to the hydrogen volume as small as 0.005% and to the weak SOI.

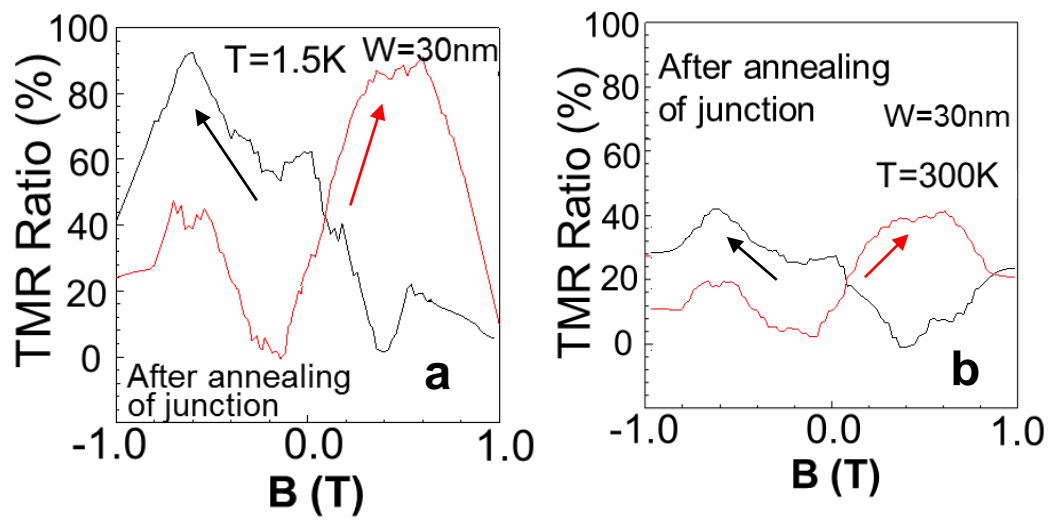


Figure 6 | TMR behaviors of the Co/SiO₂/FGNPA junction improved by annealing at (a) 1.5K and (b) 300K. The annealing at 500 °C was carried out right after depositing of SiO₂ layer on FGNPA. Improved interaction between SiO₂ layer and FGNPA yields the maximum TMR ratios mostly 5-times and 10-times larger than those in Fig.3 at T = 1.5K and 300K, respectively.

